

A Scintillating Fiber Hodoscope for a Bremstrahlung Luminosity Monitor at an Electron–Positron Collider

D.H. Brown, D.H. Orlov, G.S. Varner*, W.A. Worstell

Physics Department, Boston University, 590 Commonwealth Avenue, Boston, MA 02215

S.I. Redin†

Budker Institute of Nuclear Physics, Novosibirsk 630090 Russia

(February 5, 2008)

The performance of a scintillating fiber (2mm diameter) position sensitive detector ($4.8 \times 4.8 \text{ cm}^2$ active area) for the single bremstrahlung luminosity monitor at the VEPP-2M electron-positron collider in Novosibirsk, Russia is described. Custom electronics is triggered by coincident hits in the X and Y planes of 24 fibers each, and reduces 64 PMT signals to a 10 bit (X,Y) address. Hits are accumulated (10 kHz) in memory and display (few Hz) the VEPP-2M collision vertex. Fitting the strongly peaked distribution ($\sim 3\text{-}4 \text{ mm}$ at 1.6m from the collision vertex of VEPP-2M) to the expected QED angular distribution yields a background in agreement with an independent determination of the VEPP-2M luminosity.

I. INTRODUCTION

The VEPP-2M e^+e^- collider at the Budker Institute of Nuclear Physics, Novosibirsk, Russia is currently engaged in high precision measurements of hadron production in the 1 GeV region. These measurements are useful for reduction of the uncertainties on hadronic vacuum polarization contributions (arising from virtual photon interactions with the vector mesons ρ , ω and ϕ) to several fundamental constants of physics. Among these constants are, the muon $g-2$ value [1], the running fine structure constant evaluated at the Z -boson mass, $\alpha(M_Z^2)$ [2] [3], and the hyperfine structure of muonium [4]. The detectors CMD2 [5] and SND [6] are currently taking data in VEPP-2M to understand their systematic errors and to make preliminary measurements for these physics goals and to contribute to the planning of future high-luminosity ϕ -factories [7] [8].

In the CMD2 experiment, precise luminosity determination is performed offline by analysis of large angle Bhabha scattering events. Online luminosity determination with less accuracy is performed by small angle single and double bremstrahlung monitors. These are placed outside of CMD2 along tangents to the VEPP-2M colliding beam ring as shown in Fig. 1. The fundamental processes which generate photons from the VEPP-2M collision vertex are in descending order of cross section: single and double bremstrahlung, and two photon annihilation [9].

The CMD2 luminosity monitor (LM) systems consist

of $70 \times 70 \times 100 \text{ mm}^3$ BGO crystal scintillators and are used as rate counters [10]. The single bremstrahlung signal is difficult to distinguish from background due to beam-residual gas nuclei bremstrahlung (which shares the same strongly forward peaked QED angular distribution as the beam-beam single bremstrahlung signal) and lost beam interactions in the vacuum chamber. The latter generates photons and charged particles with a relatively broader angular distribution depending on VEPP-2M machine conditions.

The double bremstrahlung signal can be obtained by a method of coincidence between signals from LM systems on either side of CMD2. The simple coincidence signal (N_1) of the two LM systems contains actual double bremstrahlung ($\gamma\gamma$) events plus accidental (acc) coincidences from the (orders of magnitude larger rate) single bremstrahlung events: $N_1 = N_{\gamma\gamma} + N_{acc}$. The accidental coincidence rate can be measured by the coincidence signal ($N_2 = N_{acc}$) between one LM signal delayed by a few VEPP-2M beam crossings from the undelayed signal in which double bremstrahlung events cannot possibly occur. The accidental background can then be removed by subtraction of the two which isolates the double bremstrahlung events:

$$\begin{aligned} N_{\gamma\gamma} &= N_1 - N_2 \\ &= (N_{\gamma\gamma} + N_{acc}) - N_{acc} \end{aligned}$$

The problem with this method is that the small double bremstrahlung cross section implies a small number of events which means a large statistical error. This leads

*currently at Physics Department, University of Hawaii

†currently at Physics Department, Yale University

in practise to occasional negative total counts for double bremsstrahlung.

In response to the failure of rate-dependent techniques to distinguish between luminosity monitoring processes and backgrounds, the possibility to identify a signal process by its characteristic angular distribution can then be exploited. For this purpose a small diameter scintillating fiber hodoscope is employed as a luminosity monitor position sensitive detector (LMPSD) for the incidence face of the LMBGO to measure the sharply peaked profile of the photon distribution. The deviation from the expected QED angular distribution is used to measure the background to be subtracted from the total LMBGO signal. In addition, the LMPSD information provides real time visual feedback for accelerator control of the position and stability over time of the VEPP-2M colliding beam vertex (see Fig. 4).

The organization of this note is as follows. Sec. II outlines the main LMPSD components. Sec. III describes the uniformity measurements taken with a radioactive source and the performance of the LMPSD during colliding-beams operation of VEPP-2M.

II. LMPSD COMPONENTS

The LMPSD consists of a scintillating fiber package mounted to a PMT-base assembly with custom designed readout electronics. The fiber package, PMT-base assembly and readout electronics are discussed below.

A. Scintillating Fiber Package

Two scintillating fiber planes each have 24 fibers and are oriented in transverse directions to the incident photons from the interaction region of VEPP-2M. The active part of the fiber planes are 2mm diameter round radiation-hard Bicon scintillator each 6cm in length. They are index-of-refraction matched by Bicon BC-600 epoxy to 25cm long 2mm round non-scintillating clad polystyrene fibers. An aluminum frame has been constructed to fix the fibers without introducing material before or after the fiber planes in the incidence window.

Both ends of the fibers were polished. The fiber ends in the aluminum frame are held in place by clamps and adhesive to a mirrored surface, which enhances by 60 % the un-mirrored fiber light yield. The PMT-end of the fibers are held in place by a grid of 64 guide holes machined in a lucite plate. Cross talk was minimized by moving the plate within the tolerance of the bolt holes and measuring signals in a 3x3 grid of pixels with a UV-excited test fiber in the central pixel. This guide-plate is pinned to the PMT mounting plate. The entire fiber/PMT package is shown schematically in Fig. 2.

B. PMT Base Assembly

The photomultiplier (PMT) used is a Philips XP4722 segmented output electrode device with 64 individual 10 stage electron-multiplication channels. The PMT base assembly was custom designed and built in a circular array which allows each channel to be amplified separately by a current feedback operational amplifier PMI OP-160. All channels were mounted on a radial spoke (32 per side) of the circular printed circuit board. The channels on one side were rotated relative to the channels on the other to minimize cross talk through the pc board.

After initial testing the PMT gains were equalized by modifying the op-amp feedback resistors. Two raised common voltage rings supply the op-amps.

C. Mechanical Support

The fiber package is supported by attachments to the PMT mounting plate. This plate is insulating since the Philips XP4722 is used with the exterior metal ring at high voltage to maximize the PMT gain. A clear lucite fiber guide plate (with an 8x8 grid of fiber feedthrough holes) is fixed to the black plastic PMT mounting plate. The non-scintillating part of the fibers are bent equally from the two perpendicular planes in the fiber package to the PMT.

The other side of the PMT plate has a groove which accommodates the rim of a tapering (5" - 2") mu-metal shield which provides a light tight enclosure for the PMT base assembly. The cables are run out the narrow end of the mu-metal shield which is suitably taped closed for light tightness.

The amplified signal from each channel is conducted 2 meters through individual RG-174 coaxial cable to the "CODER" readout electronics. The CODER is located in a special NIM crate mounted under the CMD2 detector which converts the 64 signals to a 10 bit address for the LMPSD hit (5 bits for X, 5 bits for Y). The 10 bit address is then sent by a 4 meter 40 pin ribbon cable to a CAMAC crate.

D. The CODER Readout Electronics

The CODER electronics consists of commercial discriminators, three custom NIM modules and a custom CAMAC unit and is shown in Fig. 3. The first NIM module delivers two 5-bit values, by means of 32-bit priority encoders, for the HI and LO fibers excited in a given plane. A second such module produces HI-LO values for the other fiber plane. If HI-LO=0 then only a single fiber was hit. If HI-LO>0 then there were multiple fibers hit in the plane. (In VEPP-2M, the rate for multiple hits turned out to be quite small.) The HI-LO

modules also issue pulses useful for determining the timing of the hit.

The third NIM module is the CODER proper which delivers the $HI-LO=DIFF$ difference and the $(HI+LO)/2=MEAN$ center of the hit by means of a 2k PROM. A dip switch defining N allows the selection of events with $DIFF < N$. The signals are transformed to differential TTL to ensure that signal degradation to the CAMAC crate will not destroy LMPD information. The CAMAC unit transforms the signals back to ground relative TTL and defines the valid event condition described below.

The CODER data output consists of two 16-bit words, one for X and the other for the Y plane. Each word is issued in parallel upon a valid event defined by the logical AND between three signals: X plane OR, Y plane OR, and computer-not-busy. This signal defines the CAMAC LAM. The least significant four bits (of the 16-bit data word for each fiber plane) are the $DIFF$, the next more significant five bits are the $MEAN$ taken as the photon position, while the most significant two label the data word as X or Y . The computer program sends the $DIFF$ and $MEAN$ bits (along with the VEPP-2M beam current updated every 100th event) to a disk resident file in a form suitable for analysis software [11]. The logical AND signal of the X and Y plane ORs (without computer-busy veto) was additionally readout and sent to a CAMAC scaler.

III. LMPD PERFORMANCE

A. Calibration

Before mounting the LMPD in VEPP-2M, LMPD signal responses to illumination by a Ru^{106} source were measured to determine (and equalize) the uniformity among fiber channel responses throughout the data acquisition chain.

The 64-channel PMT-base assembly has gain variations of at least a factor of 2 while there are also 25% variations in individual fiber light yields. The discriminator thresholds in the CODER of the fiber-PMT signals provide a convenient means for equalizing the channel responses to constant illumination. Constant illumination is achieved with an uncollimated Ru^{106} source of 3.5 MeV electrons placed 15 cm away from the X and Y planes of the LMPD.

There are 4 discriminator thresholds for the 48 channels (24 for both X and Y) in the LMPD. After checking the signal response to the collimated Ru^{106} source for each channel on an oscilloscope the channels were grouped into 4 threshold groups. The LMPD was subjected to uncollimated constant illumination and the thresholds were adjusted to improve the uniformity of response across the channels. In some cases, high gain PMT channels were re-matched with low light yielding

fibers to create a more uniform response. The uniformity appears to be quite stable over long periods of operation and after complete reinstallation procedures (from one side of CMD2 to the other).

The channels tuned in this manner have yielded the photon beam position in the data presented below and appear to be acceptable. The limitation to the uniformity is determined mainly by the lack of individual channel discrimination. If this were built into the pc-board or if more discriminators were available the uniformity of the device could be improved.

B. Conversion of Photons

As depicted by small wedges on the outer radii of the bending magnets in Fig. 1, the vacuum chamber of the VEPP-2M storage ring has special photon channels with a thin (~ 1 mm) stainless steel window ($\sim 2 \times 4$ cm²) through which the bremsstrahlung photons may pass. In principle, single bremsstrahlung photons will convert to an e^+e^- pair through this chamber wall. However, earlier measurements using wire chambers determined that beam loss interactions in the vacuum chamber and other hardware in the VEPP-2M ring cause a much larger charged particle background at the luminosity monitors than the photon- e^+e^- conversion signal.

Therefore, a scintillator/PMT assembly was placed just in front of the LMPD to veto charged particles. This was implemented in the electronics by taking both of the discriminator outputs from the scintillator signal and feeding them into channel 30 and 32 in the HI-LO NIM modules. With $DIFF < 1$ event definition, this meant that a scintillator hit in those channels *and* a fiber hit in channels 1-24 would certainly yield $DIFF > 1$ and hence the event would not be issued as valid.

With photon conversions in the vacuum chamber window and *any* other charged particle background mostly removed by a scintillator veto, photon purity of the signal reaching the LMPD was significantly increased. To introduce post-scintillator conversion and thereby increase the efficiency of the LMPD several different thicknesses of tungsten plates (varying from 1 mm to 3.5 cm) were tested. In addition, the light tight enclosure built around the fiber package introduces a further 1 mm of stainless steel. After comparison of the peak value and width of the two dimensional distributions for all configurations (the largest peak results in the narrowest width because of the self-trigger of LMPD) the optimal configuration was observed to be an additional 1 mm stainless steel plate placed in front of the LMPD enclosure.

C. Colliding Beam Data

The LMPD is intended to provide position information useful for determining the angular distribution of

the single bremsstrahlung signal. In the operation of the LMPD, the photons from the VEPP-2M collision vertex are incident upon the two scintillating fiber planes located (after an e^+e^- conversion plate, see above) in front of a BGO crystal electromagnetic calorimeter. The luminosity determination by the single bremsstrahlung process can be improved by removing the deviation from the expected QED angular distribution which falls off faster than the LMPD data.

The LMPD signals were accumulated for 10k events and read out to a CAMAC memory register (CMR) by PDP-11 type and DEC VAX assembler. The signals from the CMR, were sent both to computer memory and through a Color Display Unit to an online color monitor for control room viewing, as in Fig.4. A clean collision vertex is characterized by a single bremsstrahlung peak; in comparison, noticeable changes (additional peaks) were observed with deliberate VEPP-2M orbit modifications (transverse displacement by a few mm).

The LMPD signal for VEPP-2M operation with colliding beams at energy 497 MeV per beam is shown in 3D relief for several configurations in Figs. 5-11. Fig. 5 is the LMPD signal with self XY-trigger alone; Fig. 6 is the LMPD signal in anti-coincidence with a scintillator pad-

dle in front of the LMPD to veto charged particle incidence; Fig. 7 is the LMPD/scintillator-veto signal in further coincidence with the BGO calorimeter signal above an energy threshold of 200 MeV; all have the same total number of events and for comparison have the same vertical scale. Clearly, the scintillator-veto removes charged particle background and the BGO coincidence removes remaining low energy photon background; both combinations increase the LMPD single bremsstrahlung signal relative to background. These distributions confirm earlier measurements with a multiwire proportional chamber which indicated that the beam loss background was predominantly low energy in composition and broadly distributed [10].

Without coincidence, the self-trigger of the LMPD signal alone is not sufficient to observe the QED angular distribution of the single bremsstrahlung signal; the self-trigger signal distribution is almost as populated off the bremsstrahlung peak due to the low energy background as it is on peak. Therefore, the best operating conditions of the LMPD is in conjunction with both the scintillator veto and BGO signal above threshold. This is the data which is fit by the expected QED angular distribution.

D. Fit to Quantum Electrodynamics

The final LMPD/Veto/BGO signal can now be compared with the QED angular distribution of the single bremsstrahlung process:

$$\sigma_\gamma(x, y) = \frac{d^2\sigma_\gamma}{dx dy} = \frac{\gamma^2}{2\pi} \left[E_1 \frac{1}{\left(1 + \frac{\gamma^2}{z^2} (x^2 + y^2)\right)^2} + E_2 \frac{\frac{\gamma^2}{z^2} (x^2 + y^2)}{\left(1 + \frac{\gamma^2}{z^2} (x^2 + y^2)\right)^4} \right]$$

where γ is the electron Lorentz factor, z is the distance from the VEPP-2M collision vertex to the LMPD, and x, y are the transverse dimensions of the LMPD hodoscope window. The explicit form of the dimensionless energy and threshold dependent constants E_1 and E_2 are given in Appendix A.

An online result from the LMPD requires simplification of the true QED formula in order to minimize dead time for the CMD2 experiment. A simplified form which exhibits the essential behaviour of the principal first term of the QED angular distribution is:

$$\sigma_\gamma(x - x_0, y - y_0) \simeq \frac{A}{\left(1 + a(x - x_0)^2 + b(y - y_0)^2\right)^2}.$$

The parameters a and b characterize the width of the distributions in the two dimensions and are allowed to vary in the fit. The five parameters of the fit are: amplitude A , center (x_0, y_0) and widths (a, b) of the distribution.

The procedure for determination of the background is to fit the data to the expected QED distribution only at the top part of the peak where the signal is expected to

dominate. Next, the optimized fit parameters are used to extrapolate the QED function to the tail regions where the background is expected to be larger. Such a fit (3 fibers in the x and y planes each) is shown in Fig. 8 for the data of Fig. 7; a one dimensional slice of the two dimensional distribution is shown in Fig. 9 on peak and in Fig. 10 off peak; while the fit on peak is quite good for a range of fibers included in the fit (depicted by the several curves shown), the background above the QED fit is clearly seen in the off peak slice.

By plotting the QED function with the fit parameters from the peak over the whole area of LMPD the number of total events due to the QED single bremsstrahlung process can be determined. The remaining events are considered background. A plot of the background which is the difference of the data and the full QED plot is given in Fig. 11. The relative number of events in background and QED signal for four different fit regions are presented below in Tab. I for a five parameter fit. The fit regions are defined by how many fibers relative to the maximum pixel (x_0, y_0) in the LMPD window are included in the fit.

E. Comparison of LMPSD with LMBGO and CMD2

The LMPSD results for the background in the LMBGO monitors may now be compared with results derived from independent luminosity measurements by CMD2 and LMBGO. The CMD2 luminosity measurement for Run 2729 is determined by the number of and QED cross section for Bhabha scattering events to be $\mathcal{L}_{CMD2} = N_{ee}/\sigma_{ee} = 6.2 \pm 0.12 \text{ nb}^{-1}$. The quoted error is statistical only.

The LMBGO determination of the VEPP-2M luminosity is based on a similar relation using the QED cross section for single bremsstrahlung events: $\mathcal{L}_{LMBGO} = N_{LMBGO}/\sigma_\gamma$ which for CMD2 Run 2729 is calculated to be $\sim 7.7 \text{ nb}^{-1}$. The statistical error is negligible compared to the systematic error due to presence of background which is the object under study. Comparison with the CMD2 luminosity yields a first approximation to the amount of background in the LMBGO luminosity as follows:

$$\frac{\mathcal{L}_{LMBGO}}{\mathcal{L}_{CMD2}} = \frac{\mathcal{L}_\gamma + \mathcal{L}_{bkgd}}{\mathcal{L}_{CMD2}} = 1 + \frac{\mathcal{L}_{bkgd}}{\mathcal{L}_\gamma} = 1.24.$$

It is assumed that the ideal single bremsstrahlung and CMD2 Bhabha luminosity are equal: $\mathcal{L}_\gamma = \mathcal{L}_{CMD2}$.

The ratio of background to single bremsstrahlung signal obtained in this way should be equivalent to the ratio of background and single bremsstrahlung signal obtained by LMPSD:

$$\frac{N_{LMPSD}}{N_\gamma} = \frac{N_\gamma + N_{bkgd}}{N_\gamma} = 1 + \frac{N_{bkgd}}{N_\gamma} = 1.25 \pm 0.05$$

where the ratio from Tab. I Fit 3 is shown for comparison. The systematic error is determined by variation of the QED fit region on the peak of the LMPSD data. As seen in Tab. I, the ratio of background to signal events varies from 20% to 28% for the four different fits presented there.

The implication of this result is that the LMPSD can produce a result ON-line for how much of the LMBGO signal needs to be subtracted for a more accurate luminosity measurement. The luminosity measurements from the LMBGO and CMD2 above were determined long after data taking by OFF-line processing. The LMPSD can provide its measurement of the background to signal ratio in each monitor record written to tape *during* data taking. In addition, the LMPSD-corrected LMBGO result can be simultaneously displayed ON-line. This information and the automatically refreshing visual beam

spot display from the LMPSD system are useful for shift operators to determine both the quality of beam collisions and to control more precisely how much luminosity is taken by CMD2 at each energy point of the data taking scan.

Acknowledgements

The authors would like to thank Drs. Boris I. Khazin, Andrei G. Shamov, Vladimir P. Smaktin and Dmitri N. Grigoriev of the Budker Institute of Nuclear Physics for proposing the need for the LMPSD, providing support at VEPP-2M for data acquisition and analysis of results.

APPENDIX A: QED ANGULAR DISTRIBUTION FOR SINGLE BREMSSTRAHLUNG

There are eight Feynman diagrams which contribute to the single bremsstrahlung process in Bhabha scattering: four (one radiated photon for each external particle) associated with the s channel, and another four with the t channel process. For application to photons being detected with the CMD2 luminosity monitor system, the general calculation [9] is simplified for the limit of photons emitted close to the incident beam axis and at ultra-relativistic electron energies. In this limit, only the four t channel diagrams contribute and the double differential cross section with respect to polar angle $n = \theta_\gamma = \theta E/m_e$ and photon energy ω (energy fraction $x \equiv \omega/E$) is given by [12]:

$$\frac{d^2\sigma_\gamma}{d\omega dn} = 4\alpha r_0^2 \frac{1}{\omega} \frac{n}{(1+n^2)^2} [I_1 + (I_2 + x^2) \ln(4\gamma^2 \{1/x - 1\})]$$

$$I_1 = -(2-x)^2 + \frac{16n^2}{(1+n^2)^2}(1-x)$$

$$I_2 = 2(1-x) - \frac{4n^2}{(1+n^2)^2}(1-x)$$

where r_0 is the classical electron radius.

Since LMPSD will ultimately be used in conjunction with the BGO calorimeter system which detects photons above an energy threshold ω_{th} (to remove low energy backgrounds), this expression needs to be integrated from ω_{th} to $E \equiv E_{max}^\gamma \simeq E_{beam}^e$ in order to obtain the QED angular distribution of the single bremsstrahlung photons. It is convenient to write $\omega = \omega_{th}$, $x = x_{th}$ for notation in the result below:

$$\begin{aligned} \int_{\omega_{th}}^E d\omega \frac{d^2\sigma_\gamma}{d\omega dn} &= \frac{d\sigma_\gamma}{dn} = 4\alpha r_0^2 \left[\frac{n}{(1+n^2)^2} (4A + 2B + C + Z_2) + \frac{n^3}{(1+n^2)^4} (16A - 4B) \right] \\ Z_n &= \frac{1}{n^2} (x^n - 1) \\ A &= \ln(E - \omega) + Z_1 \\ B &= \ln 4\gamma^2 \ln(E - \omega) + \ln E \ln(E + \omega) \frac{1}{2} ((\ln E)^2 - (\ln \omega)^2) + \end{aligned}$$

$$x \ln \omega - \ln E - Z_1 \ln \frac{E - \omega}{4\gamma^2} + \sum_1^\infty Z_n$$

$$C = Z_2 \ln \frac{\omega}{4\gamma^2 (E - \omega)} + \frac{1}{2} (\ln \omega - \ln E) - \frac{1}{2}$$

In order to write this in terms of the LMPSD hodoscope variables x, y it is necessary to make a small angle approximation since $x, y < 5$ cm and $z = 1.6$ m (the distance from the CMD2 collision vertex to LMPSD) and note that:

$$n = \gamma\theta \rightarrow n dn = \gamma^2 \theta d\theta \frac{d\phi}{2\pi} \simeq \frac{\gamma^2}{2\pi} \sin \theta d\theta d\phi = \frac{\gamma^2}{2\pi} dx dy$$

$$\theta \simeq \sin \theta \simeq \frac{r}{z} = \frac{\sqrt{x^2 + y^2}}{z} \rightarrow n^2 = \gamma^2 \theta^2 \simeq \frac{\gamma^2}{z^2} (x^2 + y^2).$$

Making these substitutions the result is as quoted:

$$\sigma_\gamma(x, y) = \frac{d^2\sigma_\gamma}{dx dy} = \frac{\gamma^2}{2\pi} \left[E_1 \frac{1}{\left(1 + \frac{\gamma^2}{z^2} (x^2 + y^2)\right)^2} + E_2 \frac{\frac{\gamma^2}{z^2} (x^2 + y^2)}{\left(1 + \frac{\gamma^2}{z^2} (x^2 + y^2)\right)^4} \right]$$

$$E_1 = 4A + 2B + C + Z_2$$

$$E_2 = 16A - 4B.$$

-
- [1] D.H. Brown and W.A. Worstell., Technical report, Boston University Physics Department, 1995., BNL AGS E821 $g-2$ Note # 220. *To be published in Physical Review D*.
 - [2] S. Eidelman and F. Jegerlehner., Zeitschrift für Physik, **C67**, 585 1995.
 - [3] Morris L. Swartz., SLAC-PUB-95-7001, Stanford Linear Accelerator Center, CA, 1995.
 - [4] J.R. Sapirstein et al., *Physical Review D*, **29**, 2290 1984.
 - [5] R.R. Akhmetshin et al., Preprint 95-35, Budker Insti-

tute of Nuclear Physics, Novosibirsk, Russia, 1995. *To be published in Physics Letters B*.

- [6] V.M. Aulchenko et al., Preprint 87-36, Budker Institute of Nuclear Physics, Novosibirsk, Russia, 1987.
- [7] Y.M. Shatunov et al., Technical report, Budker Institute of Nuclear Physics, Novosibirsk, Russia, 1995.
- [8] L. Maiani et al., Technical report, INFN, Laboratori Nazionali di Frascati, Italy, May 1995.
- [9] V.N. Baier et al., *Physics Reports*, **78**, 293 1981.
- [10] R.R. Akhmetshin et al., Technical report, Budker Institute of Nuclear Physics, Novosibirsk, Russia, 1995.
- [11] CERN., *PAW - Physics Analysis Workstation*, q121 edition, 1995.
- [12] S.I. Redin., Technical report, Budker Institute of Nuclear Physics, Novosibirsk, Russia, 1990.

TABLE I. Results of a five parameter fit. Total number of events is 9889. Useful result is ratio of background to signal events.

Fit	X-region	Y-region	N_{pixels}	χ^2	N_γ	N_{bkgd}	N_{bkgd}/N_γ	C
1	$x_0 - 2 : x_0 + 2$	$y_0 - 1 : y_0 + 1$	15	4.7567	7744.9	2144.1	0.2768	-
2	$x_0 - 1 : x_0 + 2$	$y_0 - 2 : y_0 + 1$	16	4.4279	8075.4	1813.6	0.2246	-
3	$x_0 - 1 : x_0 + 1$	$y_0 - 2 : y_0 + 2$	15	5.8754	7902.8	1986.2	0.2513	-
4	$x_0 - 2 : x_0 + 2$	$y_0 - 2 : y_0 + 2$	25	3.3544	8238.5	1650.5	0.2003	-

FIG. 1. Schematic of the Bremsstrahlung Luminosity Monitor Systems in VEPP-2M. Two BGO crystals $70 \times 70 \times 100mm^3$ are indicated as LMBGO, while the two planes of scintillating fibers in front of LMBGO are indicated as LMPSD.

FIG. 2. Schematic of Luminosity Monitor Position Sensitive Detector (LMPSD) hardware. Scintillating fibers are spliced to clear fibers (by index-matching epoxy) and mounted on 64 channel PMT in light tight insulating enclosure.

FIG. 3. Schematic for the LMPSD “CODER” electronics. HI-LO determination performed by four 32 bit priority encoders, while mean and differences are burned into two 2K PROMs. Events defined by zero difference are read out by CAMAC.

FIG. 4. View of LMPSD in the CMD2 Control Room shows two dimensional colour of single beam spot. VEPP-2M orbit changes visibly widen and/or produce additional beam spots.

FIG. 5. The LMPSD data with self XY -trigger alone.

FIG. 6. The LMPSD data in anti-coincidence with an upstream scintillator.

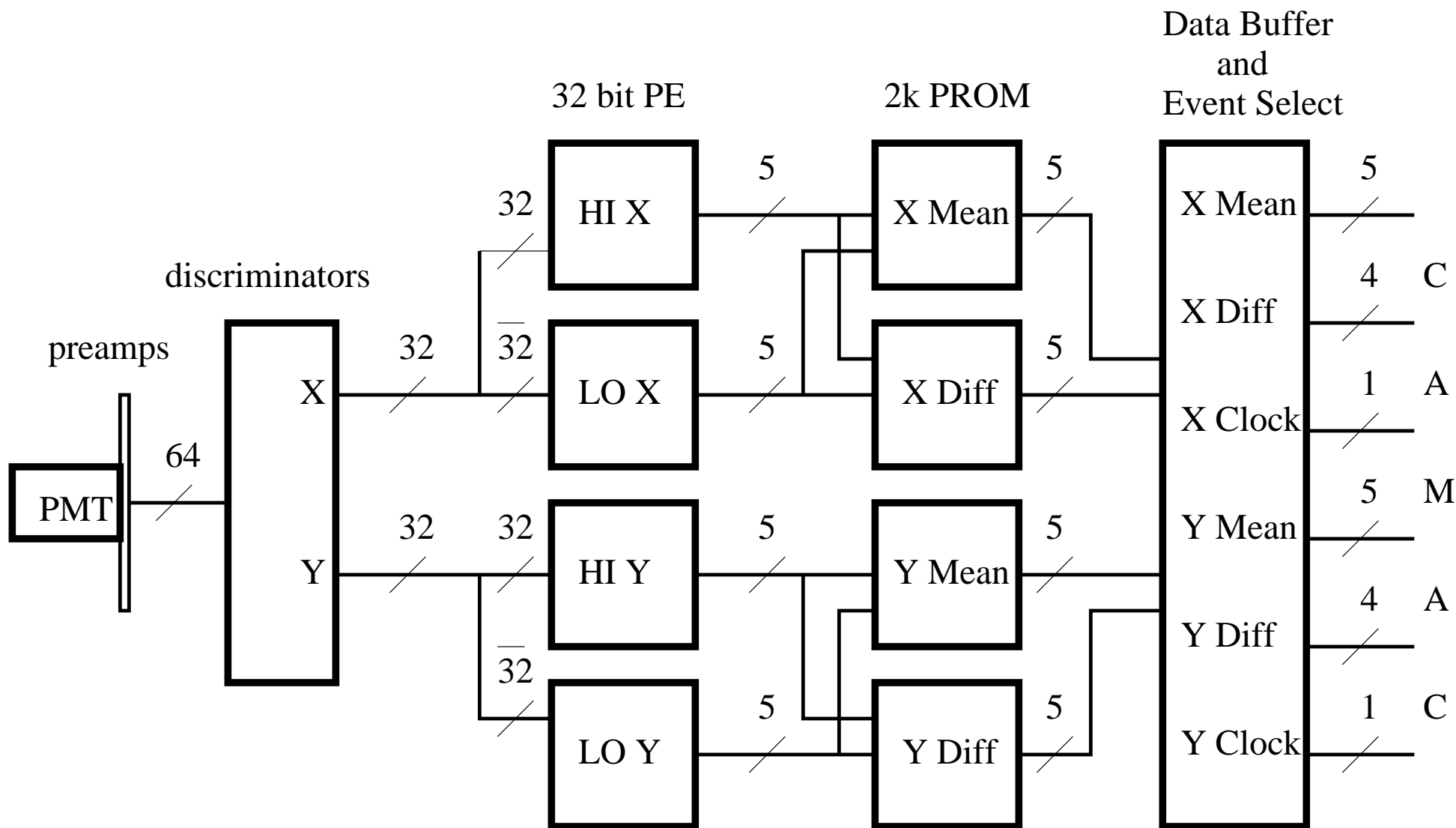
FIG. 7. The LMPSD data in anti-coincidence with an upstream scintillator and in coincidence with the BGO calorimeter above 200 MeV threshold.

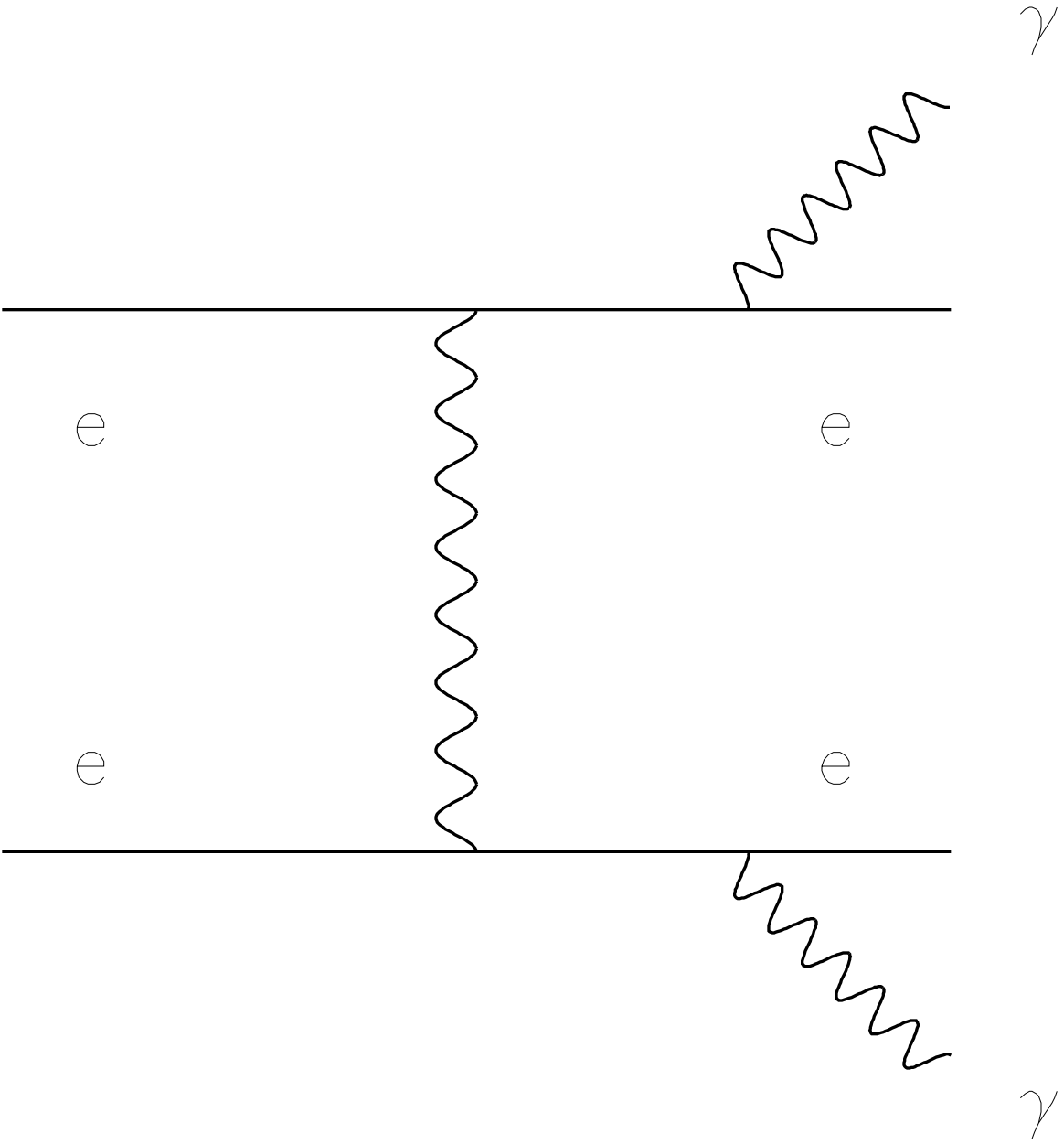
FIG. 8. The best fit of the LMPSD data with the QED angular distribution.

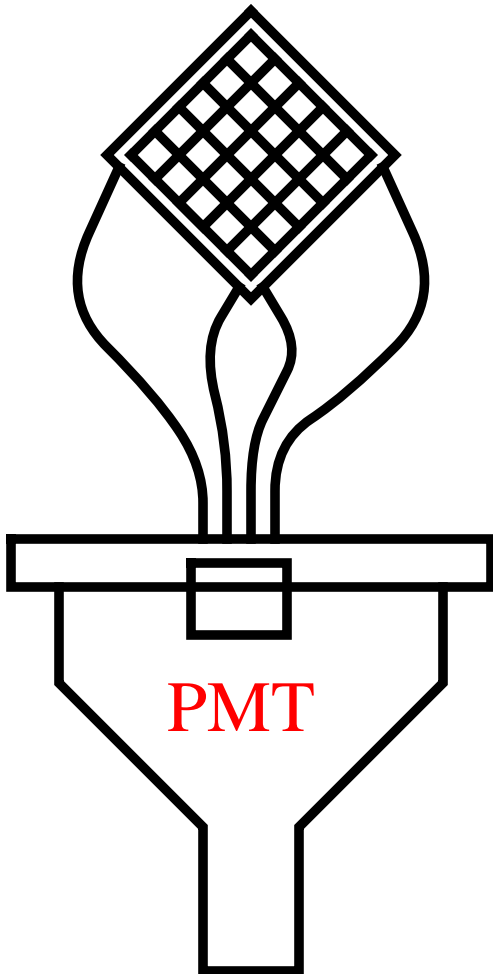
FIG. 9. A slice of the LMPSD data with fit: on peak. The many curves are for the fit regions shown in Tab. I and show agreement with the data.

FIG. 10. A slice of the LMPSD data with fit: off peak. The many curves are for the fit regions shown in Tab. I and show how much data is due to signal (under) and background (above curves).

FIG. 11. The background in the LMPSD data: difference of data with fit.







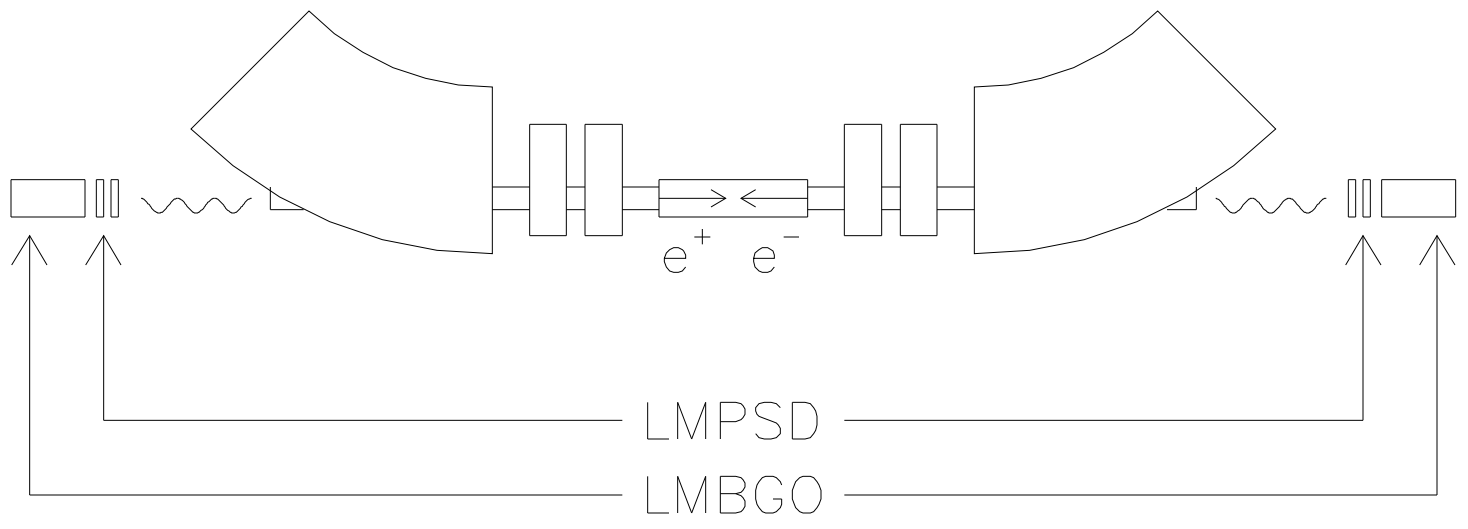
scintillating fibers

light guide fibers

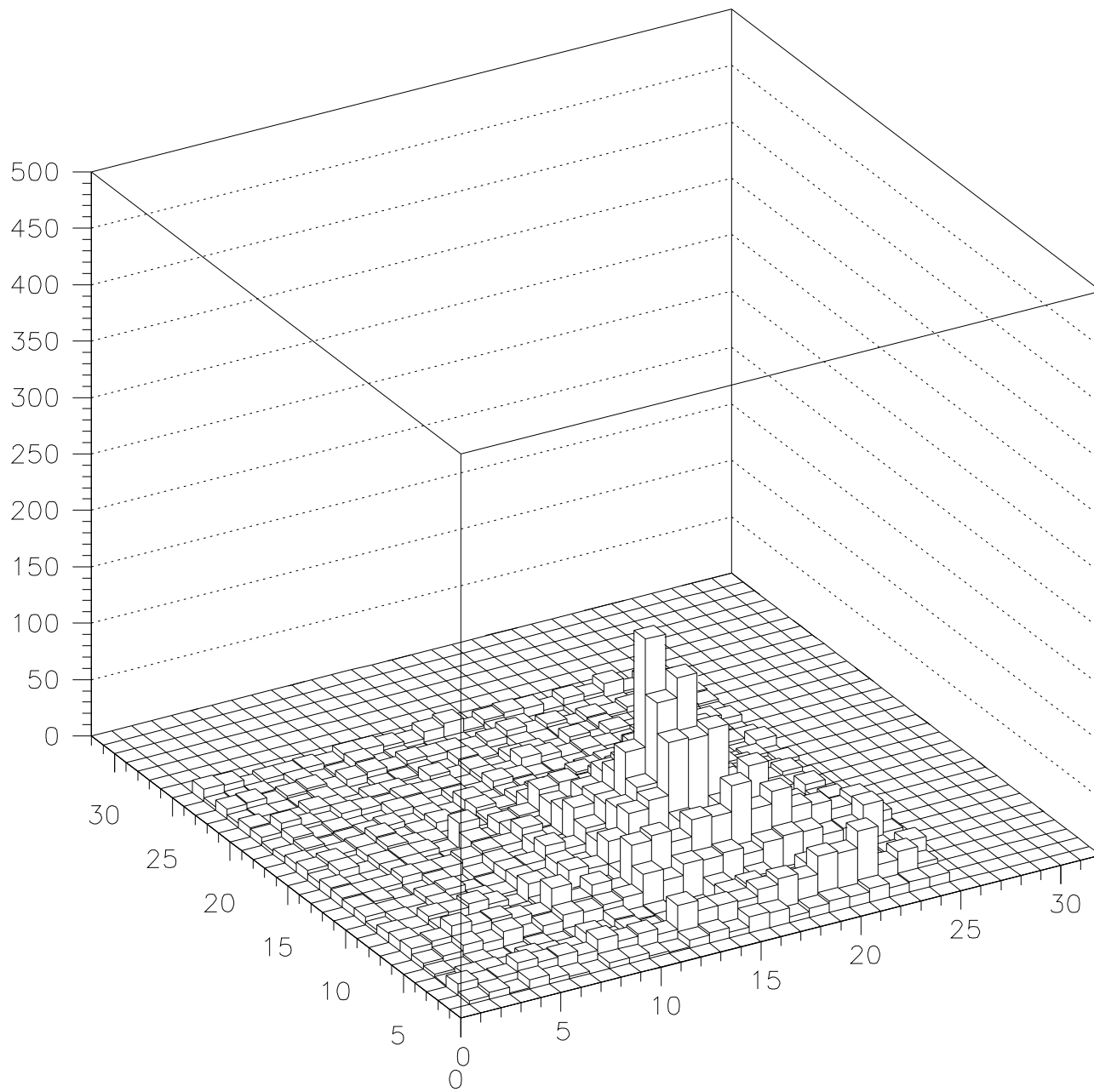
insulating plate

PMT

light tight mu metal shield

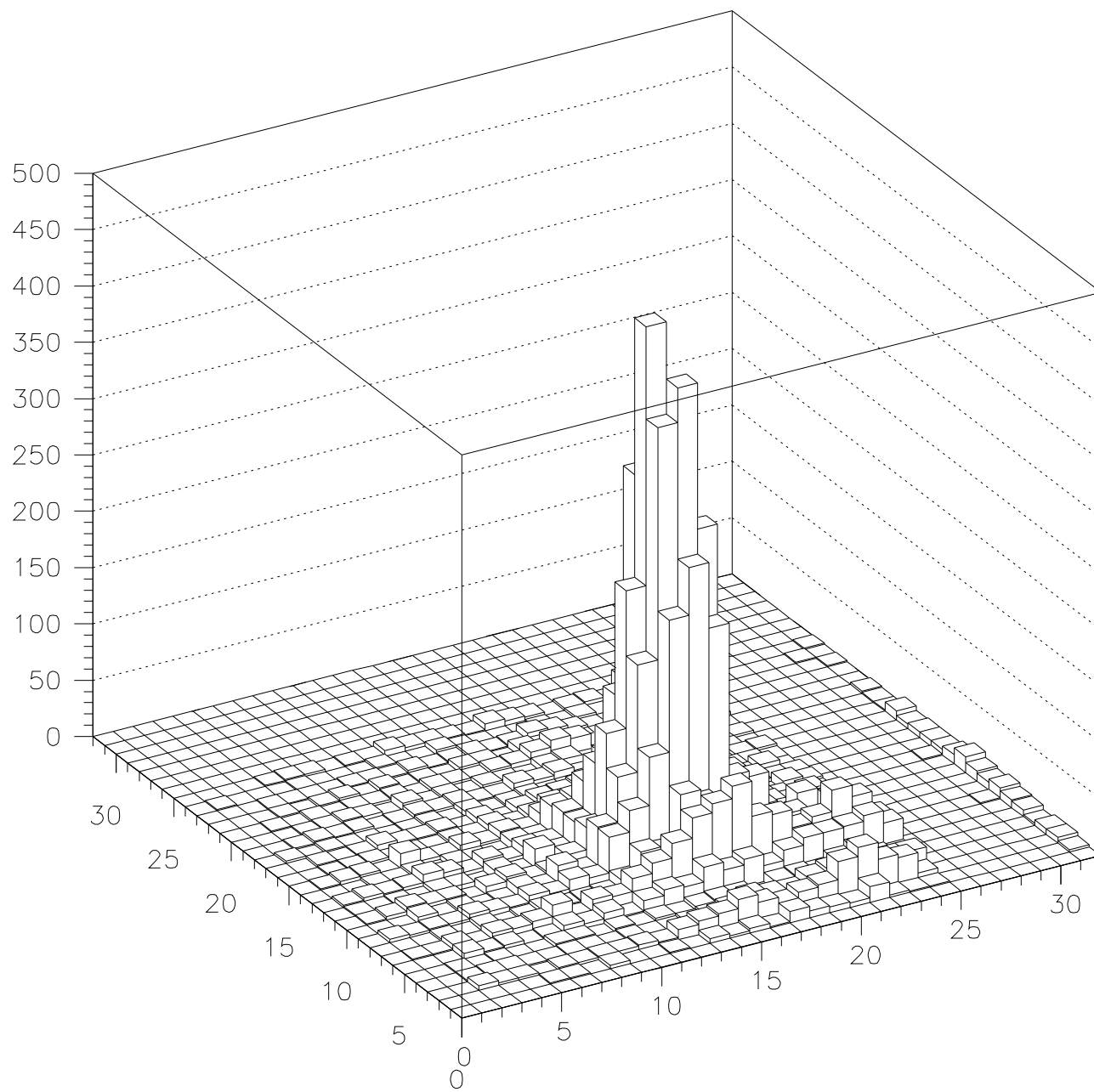


LMPSD Data - Self Trigger



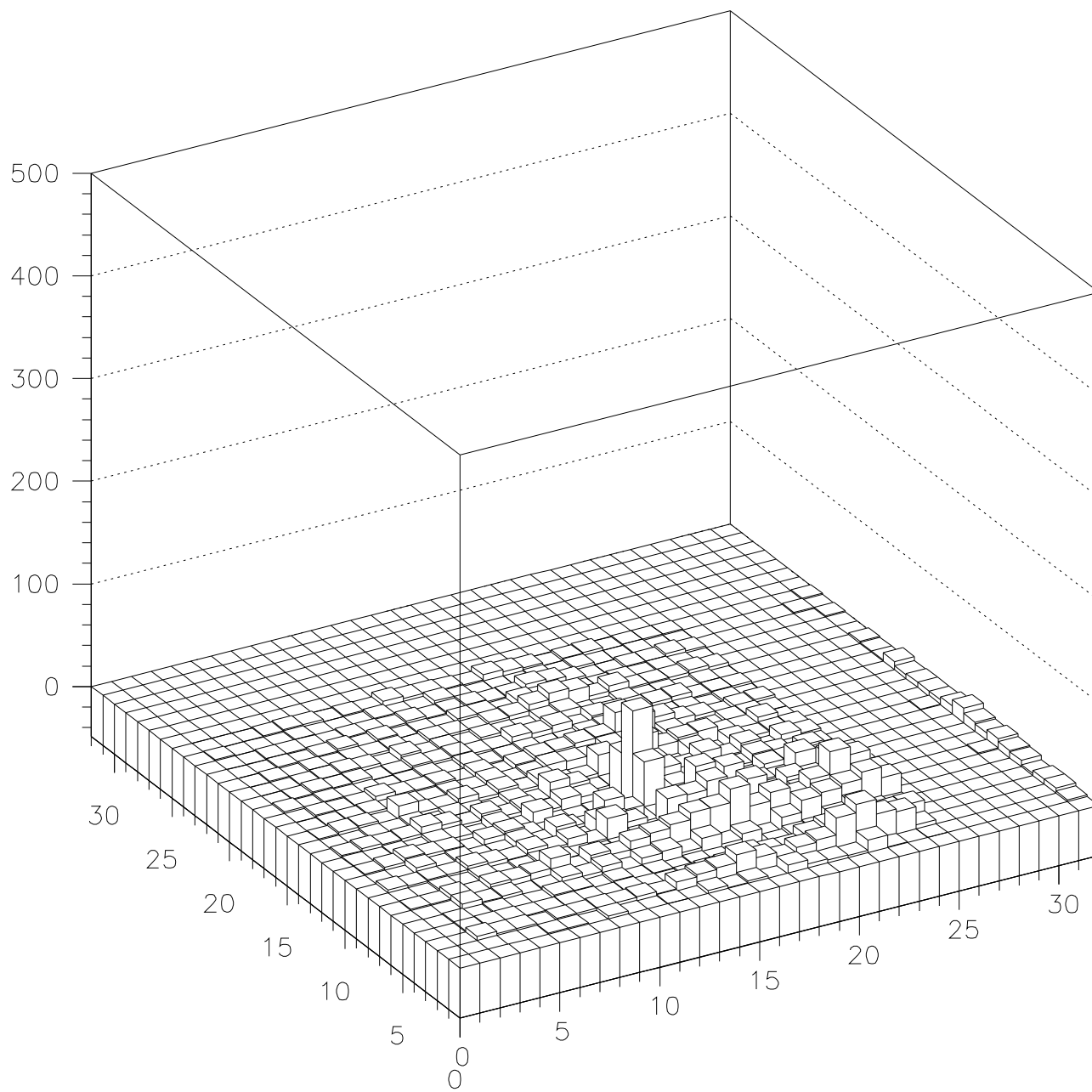
LMPSD1 X-Y HIST

LMPSD Data with Veto and BGO



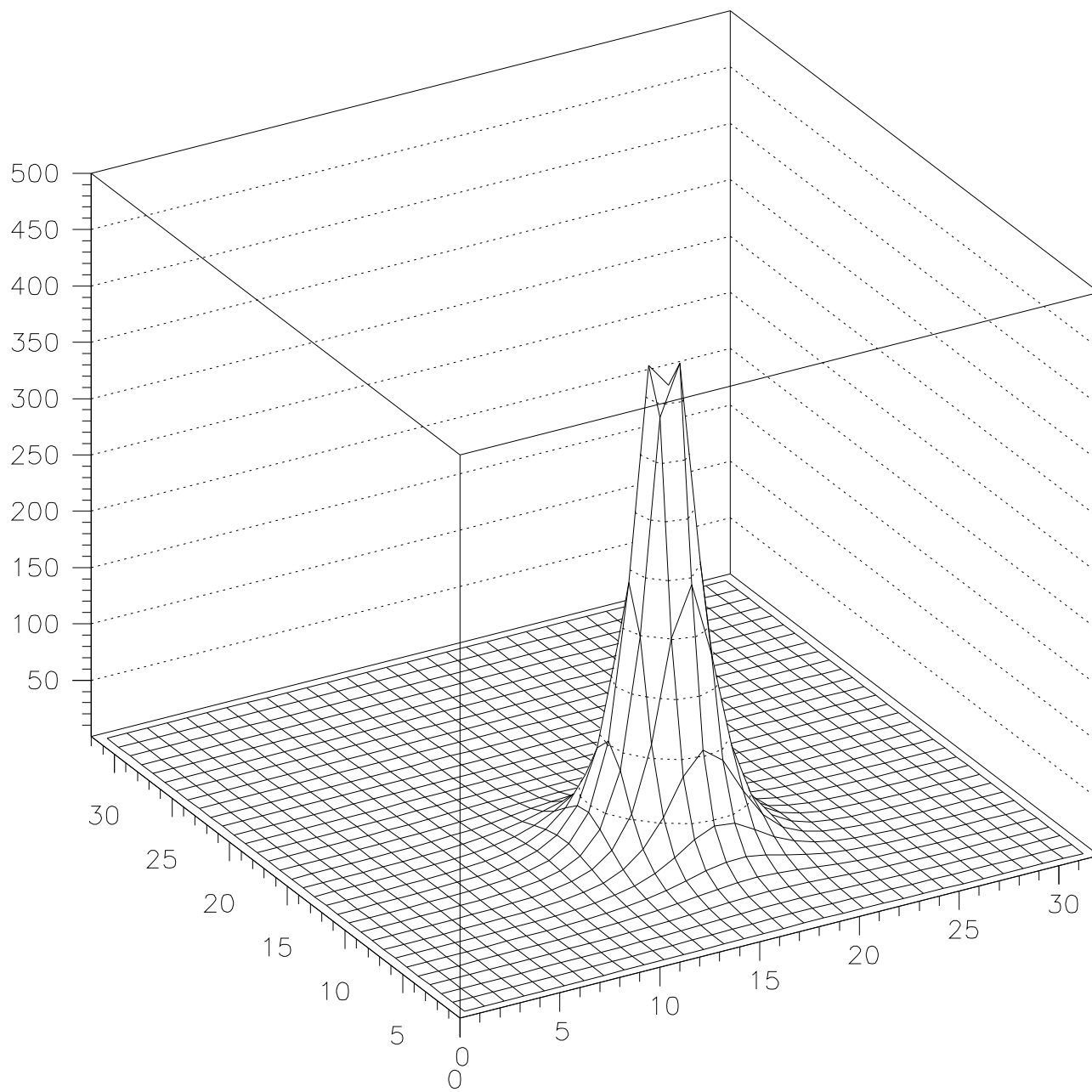
LMPSD1 X-Y HIST

$$LMPSD\ Bkgd = Data - Fit$$



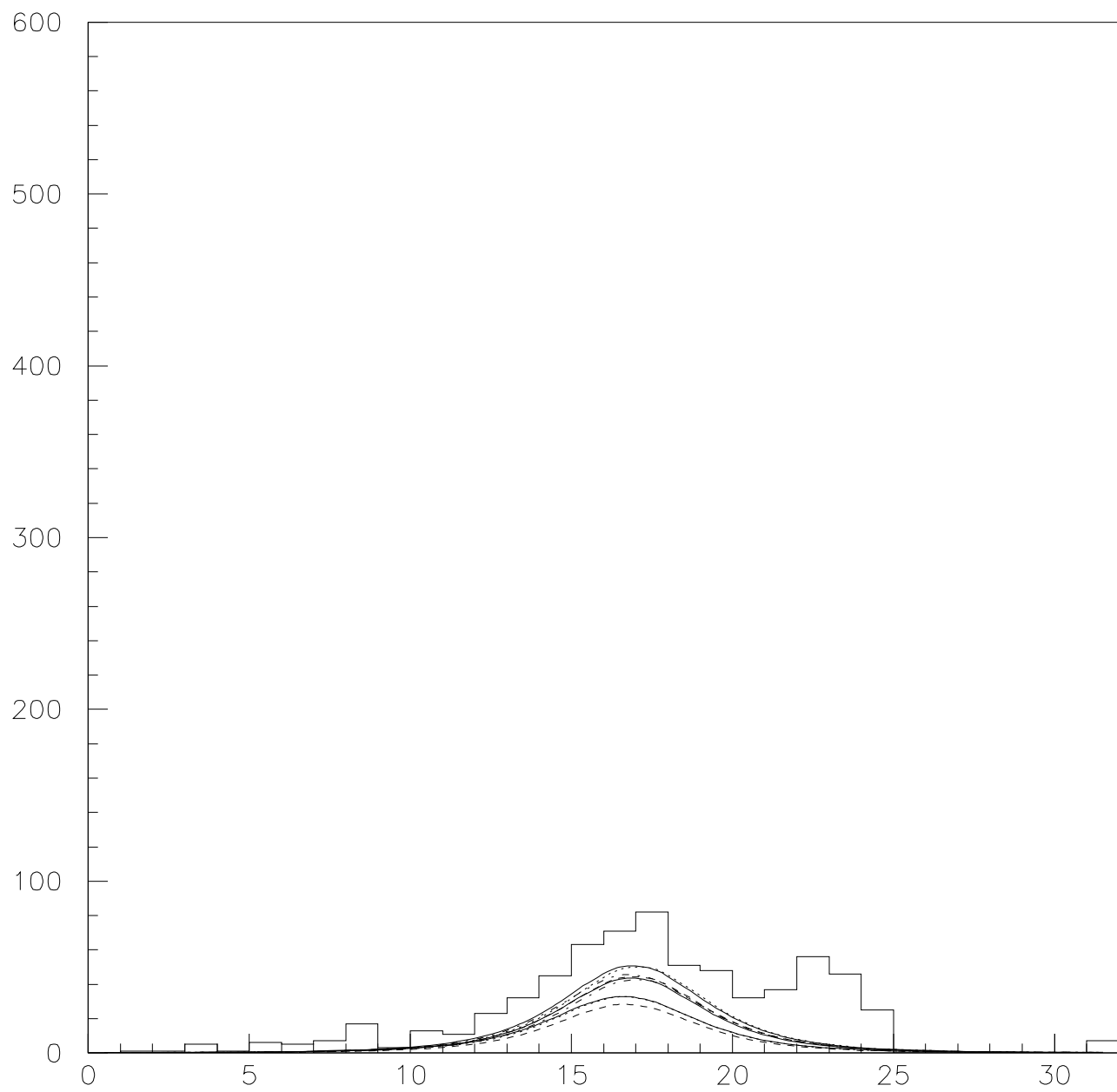
LMPSD1 X-Y HIST

QED Fit to LMPSD Data

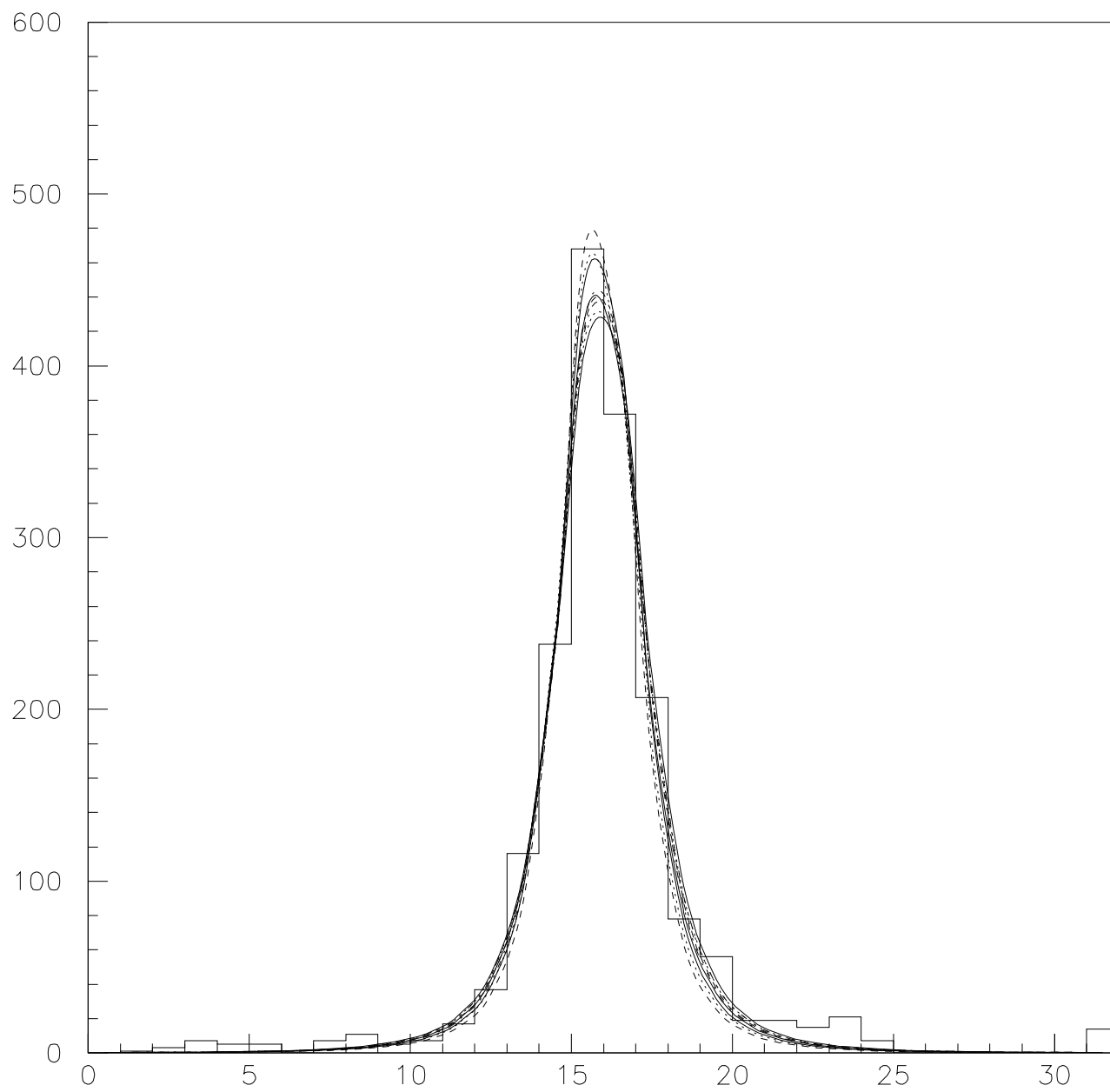


BREIT62.FOR

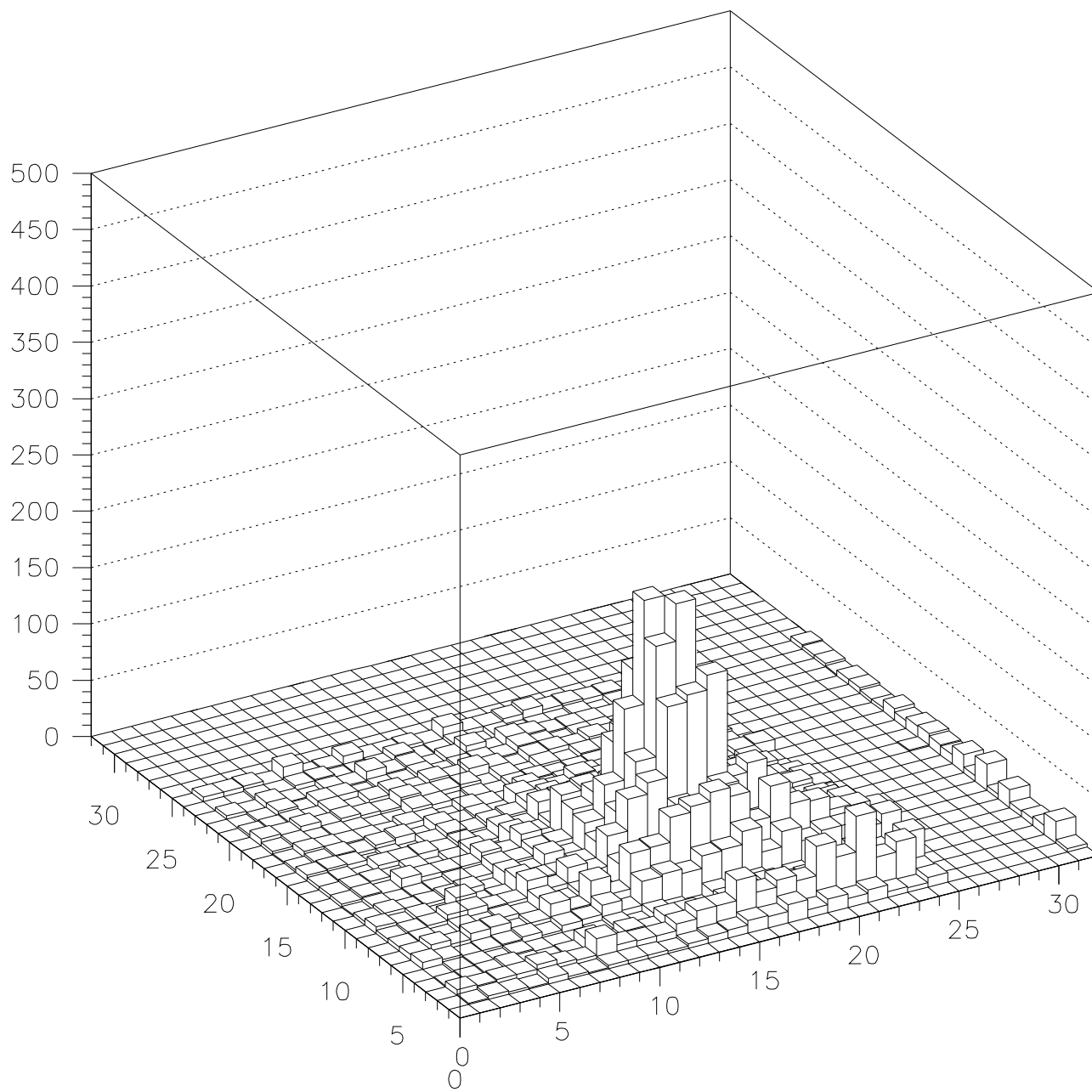
Fiber Y=7 SLIX



Fiber Y=11 SLIX

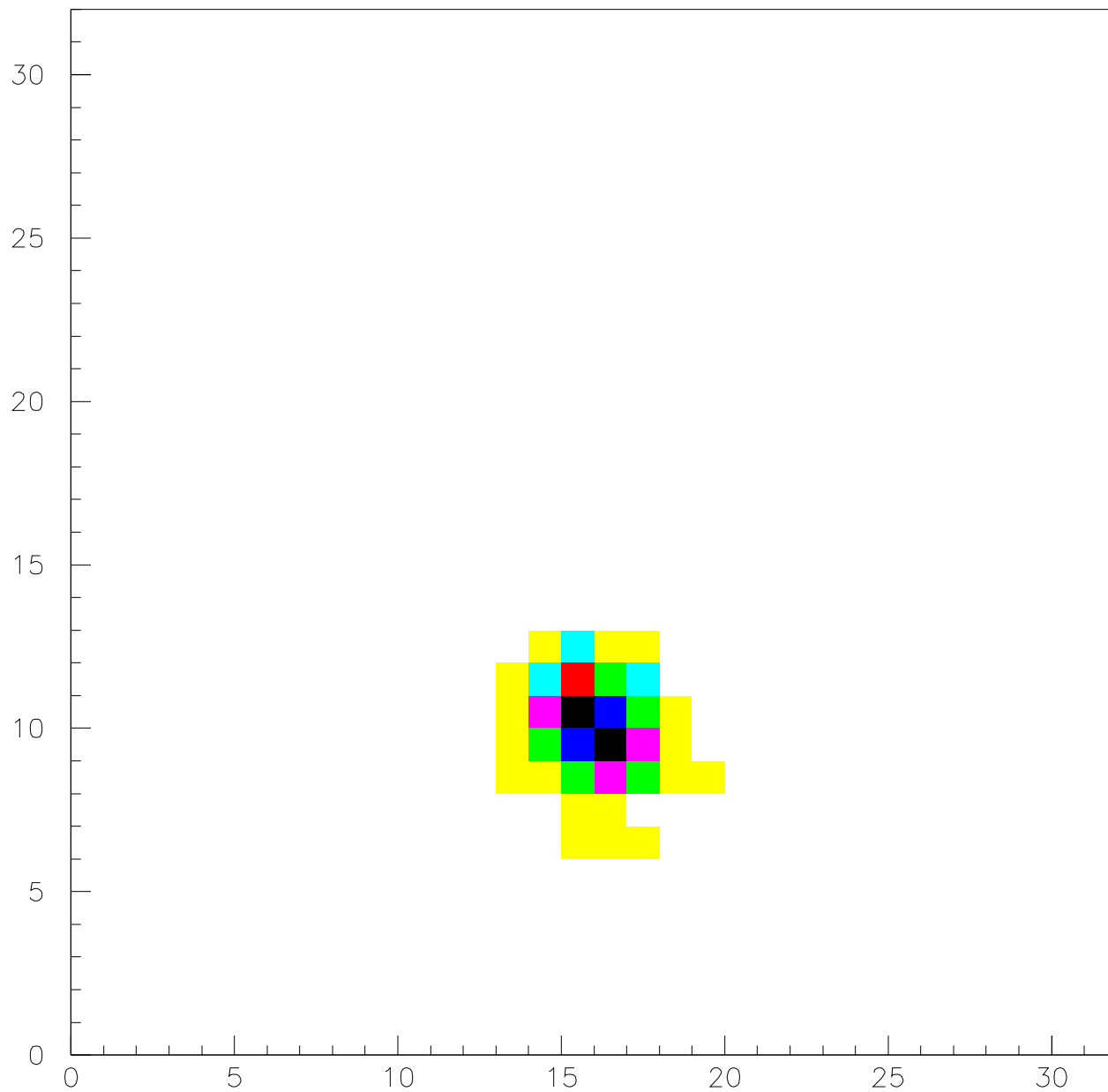


LMPSD Data with Scint Veto



LMPSD1 X-Y HIST

LMPSD Data in Shaded View



LMPSD1 X-Y HIST

